Citation: Zhaoqing Chen, Ankang Chen, Fengyuan Xie, et al. Study on the ice melting performance of prefabricated carbon fiber heating asphalt concrete pavement. *Journal of Harbin Institute of Technology (New Series)*, DOI: 10.11916/j.issn.1005-9113.25046

Study on the Ice Melting Performance of Prefabricated Carbon Fiber Heating Asphalt Concrete Pavement

Zhaoqing Chen[1], Ankang Chen[1], Fengyuan Xie[1,2], Qingyue Kong[3], Chunxue Xu[3] and Ya-na Guo[3]*

(*1. School of Civil Engineering and Architecture, Northeast Electric Power University, Jilin 132012, China;*
2. State Grid Zhejiang Electric Power Co., Ltd. Linhai Power Supply Company, Linhai 317000, China;
3. Jilin Blue View Engineering Quality Testing Co., Ltd., Jilin 132012, China)

Abstract: A prefabricated modular ice melting structure using carbon fiber heating technology is designed to address winter ice formation on asphalt pavements in cold regions. This study tests the ice melting performance of carbon fiber heating wires under different burial depths, spacing, power levels and ambient temperatures in a walk-in low-temperature environmental chamber, and determines the optimal power configurations for various environments. A multi-dimensional assessment framework is developed via the AHP-TOPSIS method by evaluating melting efficiency, construction feasibility and structural durability. Results show the optimal layout of the heating wires is 75mm spacing and 30mm burial depth; recommended power levels are 600W/m^2, 500W/m^2, 400W/m^2 and 350W/m^2 for ambient temperatures below −15℃, −15℃ to −10℃, −10℃ to −5℃ and above −5℃ respectively. Field tests reveal that with an average temperature of −12℃, 13mm snow and 500W/m^2 power, the pavement temperature reaches 2.31℃ on average after 3 h of heating, with a 0.943 snow-free area ratio, meeting practical needs. The innovative structure, with factory-prefabricated heating layers containing thermal reflective films transported to the site for asphalt pouring, avoids heat source damage in traditional cast-in-place construction and boosts construction efficiency significantly.

Keywords: prefabricated asphalt concrete pavement; carbon fiber heating wire; environmental chamber ice melting test; optimal ice melting performance; outdoor snow melting tes

CLC number: U416.2 **Document code**: A **Article ID**: 1005-9113(2026)00-0000-19

0 Introduction

When urban roads become snow-covered or, the friction between vehicle tires and the road surface is significantly reduced, leading to skidding, extended braking distances, and a potential loss of control during vehicle operation. This condition severely impacts traffic flow and may cause traffic accidents[1]. Certain slopes, curves, culverts, tunnel entrances and exits, bridge sections, and roads with winter sun blind spots on urban thoroughfares frequently become the most severely affected areas for traffic accidents following the accumulation of snow and ice[2]. Each winter, following the snow and ice, roads in these areas frequently experience repeated collisions due to delayed snow and ice removal (Fig.1), resulting in vehicle damage and casualties. Such accidents occur annually in numerous cities within cold regions[3,4].

Globally, road ice removal strategies broadly are categorized into two methods: passive and active methods. Passive methods include manual removal, mechanical operations, and ice removal agent application[5].

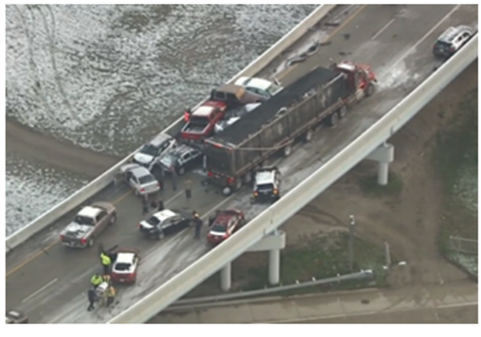

(a) At the bridge ramp location

Received 2025-09-03. Published online 2025-09-18.

* Corresponding author: Zhaoqing Chen, Ph.D, Associate Professor. Email: chenzhq2004@163.com.

(b) At the tunnel entrance

Fig. 1 Traffic accidents caused by snow and ice accumulation at different locations on the road

These conventional techniques typically require substantial human, material, and financial resources, while also causing irreversible damage to pavement structures and vegetation[6]. Active methods include new pavement ice removal techniques and thermal ice removal systems[7], etc. New pavement ice removal methods include road surface ice removal additive technology[8] and the phase-change material asphalt pavement method[9,10]. Thermal ice removal systems encompass conductive asphalt concrete[11,12] and electrically heated ice removal pavement[13], along with other types. Compared to electric heating ice melting pavement systems, conventional snow and ice removal methods typically have several disadvantages, such as high economic costs, unstable pavement stability, low ice-melting efficiency, complex construction processes, and inconsistent heat transfer performance. Currently, electric heating methods, especially those using carbon fiber heating wires, have received extensive research and application due to their cost-effectiveness, high reliability, and superior ice-melting efficiency[14,15].

The carbon fiber heating wire ice melting method typically involves installing insulated carbon fiber wires 4 – 6 cm beneath the pavement surface. When energized, these filamentous materials generate heat, to effectively melt ice and snow, a technique widely adopted in asphalt concrete pavements. However, two critical challenges persist: First, optimizing the thermal source layout and operational strategies to maximize ice-melting efficiency; Second, under the premise of ensuring simple construction, cost-effectiveness, and reliable engineering durability, the pavement structure must achieve optimal ice-melting performance[16].

Many scholars have studied the influence of heat source layout parameters (the spacing s of heating wire, the depth d), operation parameters (the heating power per unit area P, the rated power P_e) and external environment parameters (the ambient temperature T, the thickness of snow/ice t) on the effect of ice melting[17]. Liu et al.[18] experimentally investigated the effects of embedding spacing, embedding depth, heating power, heating time and ambient temperature on the surface temperature of specimens. Lim et al.[19] employed numerical simulation to analyze how the influence of heating pipe installation configuration changes on snow removal performance on road surface, and proposed a snow melting method combining urban snowfall with heating pipe power. Sadati et al.[20] investigated the thermal power requirements of airport de-icing pavement panels under various weather conditions through a combined experimental and numerical simulation approach. Ma et al.[21] conducted a sensitivity analysis of heat source layout parameters and environmental factors, revealing that the influencing factors for snow melting performance ranked as follows: embedded spacing, input power, wind speed, burial depth, and ambient temperature.

These studies explored the impact of different elements on de-icing performance and provided optimization strategies for pavement structures. However, during parameter analysis, factors such as construction difficulty, heat transfer efficiency, and pavement durability were not considered when evaluating scheme feasibility. As a result, some research findings lack practical applicability.

To address the aforementioned issues, Wang et al.[22] and Liu et al.[23] proposed that key project objectives, including time, cost, and quality, should be balanced throughout the project planning and construction phases to enhance the safety and sustainability of the projects. In the evaluation of ice melting performance, it is also necessary to comprehensively consider the comprehensive influence of various indicators. Rees et al.[24] and Liu et al.[25,26] defined a series of surface conditions to track the change process of road ice and snow area, so as to intuitively reflect the melting effect of road ice and snow. Liu et al.[27] constructed two indicators, Total Heating Time (THT) and Energy Loss Rate (LER), and carried out multi-objective optimization of input parameters based on Genetic Algorithm (GA), and finally determined the optimal heat source arrangement

parameters.

In terms of overall scheme evaluation, Ma et al.[28] proposed a multi-dimensional comprehensive quantitative evaluation method for road snowmelt performance, and innovatively constructed the comprehensive evaluation index Snow Melting Performance Coefficient (SMPC), which provided a solid scientific basis for the quantitative evaluation of electric heating pavement snow melting performance and the optimization of design parameters. Li et al.[29] analyzed the efficiency, repeatability, cost and feasibility of deicing and snow melting applications in self-deicing road systems, and proposed specific indicators for evaluating the deicing or snow melting performance of the system. Shi et al.[30] developed a thermal economic model utilizing Multi-Objective Optimization (MOO) and Genetic Algorithms (GA), addressing the dual optimization objectives of minimizing economic costs and maximizing snow-free duration. This model analyzes dynamic cost variations and snow melting processes during system operation, and has been successfully implemented at Beijing Daxing International Airport (BDIA). To achieve optimal ice melting efficiency while conserving resources and meeting rapid construction requirements, it is crucial to comprehensively evaluate how construction complexity, durability, and operational strategies influence both snow melting performance and economic benefits.

In summary, current research on asphalt concrete ice melting pavement systems primarily focuses on optimizing ice melting solutions through experimental trials and numerical simulations that account for environmental factors, pavement material types, and carbon fiber filaments burial depth and spacing. Existing construction methods almost rely on cast-in-place techniques, which present practical challenges in engineering applications. These challenges include complex construction processes, slow installation speeds, frequent displacement of carbon fiber filaments from asphalt surfaces by vehicle traffic, absence of thermal reflective layers in structural designs, low energy efficiency, and suboptimal ice melting performance. These issues significantly hinder the industrial application of carbon fiber snow/ice melting technology in road engineering projects.

To address these challenges, this study developed a prefabricated modular asphalt concrete ice melting pavement structure utilizing carbon fiber heating technology. Through laboratory tests in walk-in low-temperature chambers, we evaluated the ice melting performance of carbon fiber heating wires under varying burial depths, spacing intervals, power outputs, and ambient temperatures, identifying optimal operating power levels for different environmental conditions. Considering the interplay between ice-melting efficiency, construction feasibility, and structural durability, we proposed a multi-dimensional evaluation framework employing the AHP-TOPSIS method to assess performance metrics. The analysis identified the most effective solution, which was validated through fieldapplication trials demonstrating its practical effectiveness.

1 Ice Melting Structural Design

The prefabricated integrated ice melting pavement structure is shown in Fig. 2(a), consisted of an asphalt concrete surface layer, a concrete base layer, and a subbase layer. A heating layer structure is placed above the concrete base layer. The asphalt concrete surface layer uses AC13 cold-mixed asphalt concrete with 6% steel slag by volume to enhance thermal conductivity[31]. The concrete base layer employs C40 concrete (mix ratio shown in Table 1).

Meanwhile, during the preparation of the model, we carried out a maintenance work on the prepared specimens for 28 d. Compressive strength tests and flexural strength tests revealed that the specimens achieved a compressive strength of 49.7 MPa and a flexural strength of 4.67 MPa, meeting the ideal mechanical performance requirements, which means its anti-deformation ability and durability in long working environment.

After positioning the sections, fine adjustments were performed using hoisting machine to ensure uniform seam width that surface height differences met specifications. The final assembly of sections was then completed according to the designed connection method. Once all prefabricated plates have been installed and debugged, the surface concrete was chiseled to increase the surface friction, improve the anti-slip and anti-rushing properties, and enhance the bonding with the asphalt surface layer. Following the installation and inspection of all precast sections, the asphalt concrete surface layer was laid on the precast base using a paver, and then compacted with rollers.

Table 1 C40 concrete mix ratio

Materials	Use level
Cement	330kg
Water	132kg
Sand	654kg
Aggregate	1384.72kg
Water reducer	1.65kg

Fig.2(b) shows the schematic diagram of the heating layer's ice melting structure, which is 8 mm thick and primarily consists of carbon fiber heating wires, a steel mesh frame, thermal reflective membrane, and power supply cables. The steel mesh frame used HRB300 Φ8 steel bars, with the specifications of carbon fiber heating wires detailed in Table 2. HRB300 steel reinforcement mesh was incorporated into the base layer of the designed ice-melting pavement to secure carbon fiber heating elements and prevent displacement. The cable was separated from the thermal reflective film during pouring or use, preventing direct contact that could cause damage.

During pouring, concrete was used to fill the gaps between them to ensure that the heated structure was tightly bonded with the surrounding material. The base asphalt concrete pavement panels were prefabricated in the factory and cast and fully vibrated by automated equipment to ensure that the heating structure was closely bonded with the surrounding asphalt mixture. The prefabricated asphalt concrete pavement slab was embedded with a steel mesh as the reinforcement material, which not only played a dual role of heat transfer and enhancement, but also greatly improved the overall bending strength and stiffness of the module, effectively resisting the stress and deformation generated in the lifting and transportation process. The heating system was embedded within the asphalt surface layer as prefabricated concrete components, which were pre-manufactured and cured in factories. A thermal reflective membrane was installed inside to ensure heat transfer from the carbon fiber wires only upwards during melting, preventing downward heat loss and significantly improving thermal efficiency.

After curing, the ice-melting structure was transported to the construction site for asphalt concrete overlay pouring. Compared with the construction method of prefabricated cast-in-place ice-melt pavement, this construction method can avoid the damage of heat source caused by construction to the greatest extent, and the construction efficiency of ice-melt pavement can be significantly improved through the prefabricated assembly construction method. The ice melting pavement utilized a modular plug-in design, where each prefabricated module was pre-embedded with standardized waterproof connectors.

During installation, adjacent modules could be quickly connected by pre-installed waterproof cables, completing the electrical circuit seamlessly. As shown in Fig 2(b), the ice melting pavement utilized a modular plug-in design, where each prefabricated module was pre-embedded with standardized waterproof connectors. During installation, adjacent modules can be quickly connected by pre-installed waterproof cables, completing the electrical circuit seamlessly. The entire power supply (including electric source, temperature sensor and voltage regulator) was transmitted through cable busways embedded along the roadside, ultimately reaching power sources located on road shoulders or central medians. The design collects the ambient temperature data through the temperature sensor, and adjusts the corresponding heating power accordingly to achieve targeted ice melting operation.

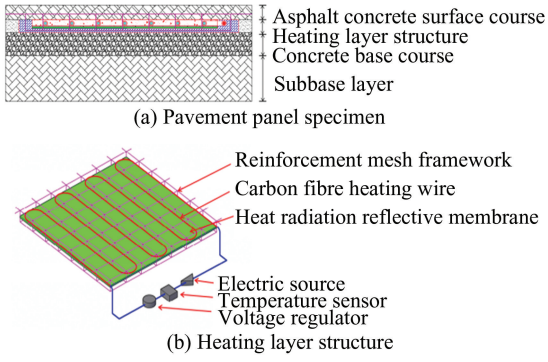

Fig. 2 Schematic diagram

Table 2 Carbon fiber heating wire parameters

Diameter	Product model	Electric resistance	Thermal efficiency	Rated line power	Tensile strength
5mm	48K	9Ω/m	>98%	35W/m	3.5GPa

The ice melting pavement structure in this study adopts the prefabricated construction method. Compared to the traditional technology, the key points of construction quality control need to be

supplemented as follows: (1) The conductivity and heating power of carbon fiber wire must be strictly tested to ensure that the resistance per unit length is not less than 6 Ω/m and the heat transfer efficiency is more than 98%; (2) The cable burial distance shall not be less than 6 times of the diameter, and the maximum burial distance shall not exceed 70 cm; (3) The heating wire spacing is not less than 30mm, not more than 100 mm; (4) The protective layer of carbon fiber heating wire has a temperature resistance range of −60℃ to 250℃ and good flexibility; (5) The reflectivity of thermal reflective film to thermal energy exceeds 95%; (6) The reinforced steel mesh material is HRB300, and the diameter of the steel bar is not less than 6mm; (7) The maximum water-cement ratio is 0.44, and the minimum cement consumption is 320 kg/m^3, the sand ratio should be between 38% and 50%; (8) Add steel fiber according to the volume ratio of concrete, not less than 3% yet not more than 8%.

2 Walk-in Low Temperature Environmental Ice Melting Test

2.1 Experimental Design

2.1.1 Test purpose and case

The purpose of the low-temperature environment storage ice melting test is to study the melting performance of carbon fiber heating wires under various conditions, including different burial depths, spacing, power levels, and environmental temperatures. The goal is to determine the appropriate power settings for various environmental temperatures.

Road ice melting method generally consists of two phases: the preheating phase and the active ice melting phase. The preheating phase, which typically lasts for 1 h following the activation of power, fulfills three primary functions: (1) It ensures uniform heating of pavement materials to prevent cracking; (2) It prevents sudden overloading from rapid temperature increases in carbon fiber strands; (3) It raises the temperature of the pavement structure to maintain thermal stability throughout subsequent ice melting operations. This phase also optimizes energy efficiency for improved effectiveness. The active ice melting phase, which extends from the end of preheating until most ice and snow have melted, is usually required to be completed within 2 h.

Based on existing research findings from Refs[32−34], this study selected several groups of burial depths and spacing intervals with relatively high ice melting efficiency as preliminary configurations for carbon fiber heating wires in the test, aiming to investigate their effects on melting efficiency. The specific configuration is detailed in Table 3, with specimen numbers labeled A−F (totaling 6 groups). The heating wires were buried at depths of 30 mm and 50 mm, with spacing intervals set at 50 mm, 75 mm, and 100 mm, respectively.

Table 3 Specimen number and heating wire arrangement parameters

Specimen number	Burial depth of heating wires (mm)	Spacing of heating wires (mm)
A	50	75
B	30	75
C	50	100
D	50	50
E	30	100
F	30	50

The specimens were prepared according to the secondary highway standard. Referring to Ref.[35] and considering the test requirements, the dimensions of pavement panel specimens were determined as a rectangular prism of 600 mm in length, 600 mm in width, and 200 mm in height, as shown in Fig.2.

Beyond meeting standard requirements, the test specimen must keep the cost of ice melting pavement below 400 yuan/m^2, with annual maintenance costs not exceeding 35 yuan/m^2. Additionally, under snow accumulation thickness of no more than 15 cm, the entire ice melting process should take no longer than 3 h. Furthermore, by adjusting input power, the carbon fiber heating element achieves controllable thermal output, enabling flexible power adjustment according to varying ambient temperatures.

Under the condition that the above requirements are met, the fabrication of specimens A−F begins. The fabrication process of the test specimen includes: formwork processing, pouring concrete for the lower part of the heating structure, laying the thermal reflective membrane, and installing the steel mesh with heating wires. After the concrete of the heating structure solidifies, asphalt concrete surface layer is poured. The specimen undergoes 28−day curing under standard conditions before conducting the heating test. The workflow diagram of the specimen fabrication process is shown in Fig.3.

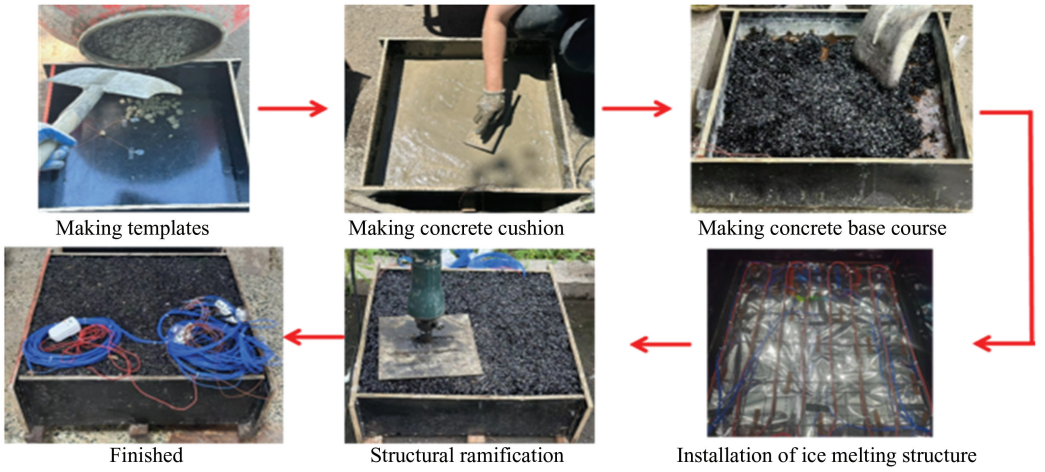

Fig.3 Flowchart of the specimen making process

During construction, the prefabricated heating layer structure was first placed on the concrete bedding. Subsequently, space for laying power cables was reserved, followed by concrete pouring. Finally, asphalt concrete was compacted.

2.1.2 Measurement point layout and experimental equipment

Temperature measurement points were strategically arranged on the surface of the heating structure specimen and at multiple locations along the heating wire to systematically track temperature variations across different temporal intervals and spatial positions. The arrangement and numbering of temperature measurement points are shown in Fig. 4. Fig.4(a) shows the surface measurement points of the specimen, and Fig.4(b) shows the measurement points near the heating wire in the heating structure.

The temperature measuring equipment is a thermocouple temperature sensor, as shown in Fig.5. Its function is to measure the temperature of the surface of the specimen and the surface of the carbon fiber heating cable in real time. The model is K type 2 * 0.5 mm, and the temperature range is −50℃ ~ 200℃.

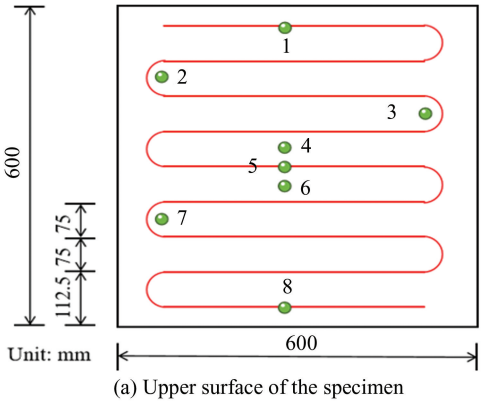

(a) Upper surface of the specimen

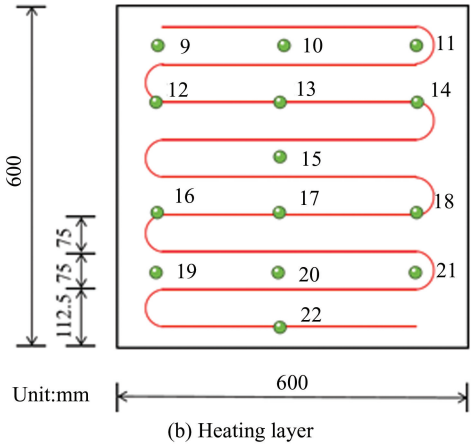

(b) Heating layer

Fig. 4 Schematic diagrams of temperature measurement point arrangement and number

Fig.5 Temperature sensor

The temperature collector used is JINKO JK5000-96 with 96 channels. Its measurement range spans from −200℃ to 1800℃, with a sampling frequency of 1s/time. The recording interval is arbitrarily adjustable between 1 and 9999s. The collected temperature includes the internal and surface temperatures of concrete, as well as ambient

temperature.

The indoor test was carried out in a walk-in environmental chamber equipped with a temperature control system. Chamber, model HY-TH-34, has a simulated environmental temperature range from −40℃ to 85℃, and the test temperature was set between −15℃ to 5℃.

In order to adjust the voltage of carbon fiber heating cable and control the input power, STG-3000 W AC voltage regulator was installed. Its rated voltage is 220 kV, adjustable voltage is 0−300 V, and the maximum power is 3000 W. The arrangement of the above test equipment and specimens is shown in Fig. 6.

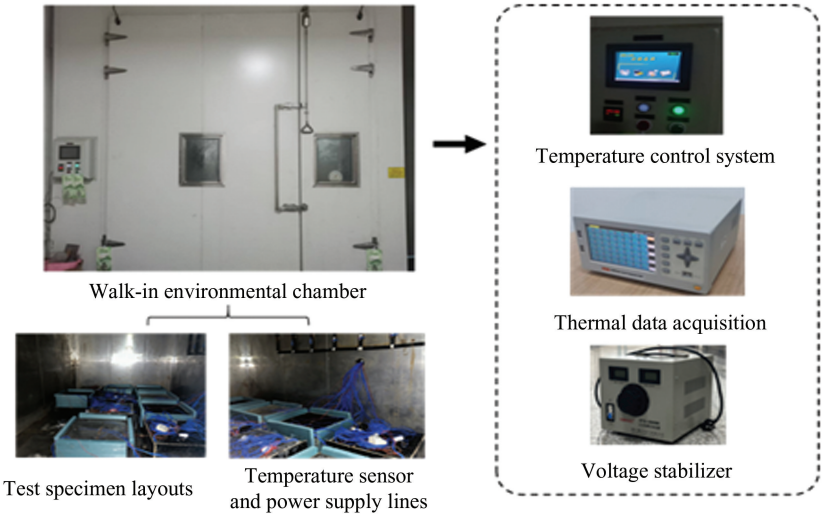

Fig.6 Layout and equipment of asphalt concrete pavement ice heating test

2.1.3 Ice melting performance indicators

The performance indicators of ice melting are divided into ice melting effect indicators, construction difficulty indicator and durability indicator.

(1) Ice melting effect indicators. Ice melting effect indicators include snow-free area ratio A_r[36], mean temperature μ of all test points on the surface of the specimen, standard deviation σ and temperature coefficient of variation cv[37,38]. The definition of the snow-free area ratio A_r is shown in Eq. (1).

$$A_r = \frac{A_f}{A_t} \tag{1}$$

where, A_f is the snow-free surface area of the specimen, A_t is the surface area of the specimen. When $A_r = 1$, it means that all the snow is completely melted. When $A_r = 0$, it means that the road surface is completely covered by snow.

The mean value of the temperature at all measurement points on the test surface μ is defined as Eq. (2):

$$\mu = \frac{\sum_{i=1}^{N} x_i}{N} \tag{2}$$

where, N is the number of measurement points, x_i is the temperature value of the measurement point i. The higher the mean value, the better the heating effect per unit time.

Standard deviation σ defined as Eq. (3):

$$\sigma = \frac{\sum_{i=1}^{N} (x_i - \mu)^2}{N} \tag{3}$$

Temperature coefficient of variation T_{cv} is defined as Eq. (4):

$$T_{cv}(t) = \frac{\sigma}{\mu} \tag{4}$$

The temperature variation coefficient T_{cv} reflects both the heating effect and the uniformity of temperature distribution. A smaller T_{cv} indicates smaller temperature differences among the monitoring points on the pavement surface, implying a more uniform heat distribution of the heating system. This ensures the absence of local overheating or overcooling, resulting in a stable melting performance.

(2) Construction difficulty and durability indicators. From the perspective of construction difficulty and durability, when the heating wire spacing becomes smaller and the burial depth shallower, the construction difficulty increases while

durability decreases. Conversely, when the heating wire spacing increases and the burial depth shallower, construction difficulty decreases while durability improves. In practical engineering applications, both low construction difficulty and good durability are required. Therefore, two specific indicators are defined: the extremely large indicator C_d (construction difficulty) and the extremely small indicator C_e (durability), which respectively characterize the construction difficulty and durability of specimens A-F. The calculation formulas are as follows:

$$C_d = \frac{1}{s} \tag{5}$$

$$C_e = \frac{1}{d} \tag{6}$$

where, s is the spacing of heating wire and d is the burial depth.

2.1.4 Determination of optimal layout scheme

In multi-criteria decision-making, determining index weights is a crucial step, as it directly determines the influence of each evaluation index on the final decision. Inaccurate or unreasonable weight allocation can lead to incorrect ranking and poor decision.

Traditional evaluation methods such as Analytic Hierarchy Process (AHP) and TOPSIS exhibit inherent limitations: AHP is overly subjective, while TOPSIS is sensitive to initial weights. To address these shortcomings, this study develops an integrated weight system for ice-melting performance indicators using the AHP-TOPSIS hybrid approach. This methodology overcomes the limitations of single-method approaches, reduces the excessive subjectivity of AHP, resolves the weighting source issues in TOPSIS, and demonstrates enhanced interpretability with broad applicability. The specific implementation steps are as follows:

(1) Determine the structure hierarchy. The ice melting performance indicators, A_r, μ, σ, T_{cv}, C_d and C_e, are the criterion layer, the ice melting performance score of arrangement scheme A-F is the target layer, and the arrangement patterns of carbon fiber heating wires in schemes A-F are designated as scheme layers.

(2) Data standardization. Assume that the indicator data matrix of the evaluation scheme is:

$$\boldsymbol{X} = \begin{bmatrix} X_{11} & \cdots & X_{1n} \\ \cdots & X_{ij} & \cdots \\ X_{m1} & \cdots & X_{mn} \end{bmatrix} \tag{7}$$

where, X_{ij} represents the data of the j indicator in scheme i, and m and n are the number of schemes and indicators respectively.

Before calculating the weight, the dimension influence of extremely large indicators and extremely small indicators is eliminated respectively by Eq. (8) and Eq. (9), and the standardized matrix $\boldsymbol{X'}$ is obtained.

$$X'_{ij} = \frac{X_{ij} - \min(X_j)}{\max(X_j) - \min(X_j)} \tag{8}$$

$$X'_{ij} = \frac{\max(X_j) - X_{ij}}{\max(X_j) - \min(X_j)} \tag{9}$$

where, X'_{ij} represents the standardized value of the j indicator in scheme i.

(3) Calculate indicator weights. Based on the criterion layer snowmelt performance index, the importance judgment matrix between indicators is constructed and the consistency test is carried out, so as to obtain the weights of ice-melting performance indexes A_r, μ, σ, T_{cv}, C_d and C_e.

The consistency test is carried out by the following equation, and the consistency test is passed when the CR value is less than 0.1:

$$CR = \frac{CI}{RI} \tag{10}$$

where, CR represents the consistency ratio; CI is the consistency index of the judgment matrix, whose value is calculated according to Eq. (11); RI is the random consistency index, which takes values according to Table 4.

$$CI = \frac{\lambda_{max} - n}{n - 1} \tag{11}$$

where, λ_{max} is the maximum eigenvalue of the judgment matrix, and n is the number of criteria layer indicators.

Table 4 *RI* value

n	1	2	3	4	5	6	7	8	9
RI	0	0	0.58	0.90	1.12	1.24	1.32	1.41	1.45

After passing the consistency test, the eigenvector $\boldsymbol{T} = [t_1, t_2, \ldots, t_n]^T$ corresponding to the maximum eigenvalue can be obtained. The eigenvector T is normalized to obtain the index weight vector $\boldsymbol{W} = [w_1, w_2, \ldots, w_n]^T$.

(4) Generate random weights. Based on the reference weight $\boldsymbol{W}$, random numbers are generated within a certain range to transform the original weight value and obtain the random weight $\boldsymbol{W'}$:

(5) Establish weighted decision evaluation matrix. Based on the generated random weight $\boldsymbol{W}'$ and standardized matrix $\boldsymbol{X}'$, the standardized weighted matrix $\boldsymbol{V}$ is calculated, and then the positive and negative ideal solutions V^+ and V^- are obtained;

$$\boldsymbol{V} = \boldsymbol{X}'_{ij} \cdot \boldsymbol{W}' \tag{12}$$

$$V^+ = \max\{V_{ij}\} \tag{13}$$

$$V^- = \min\{V_{ij}\} \tag{14}$$

(6) Calculate the score of the scheme. The distance D^+ and D^- between each scheme and V^+ and V^- are calculated respectively, and then the scheme score is calculated according to D^+ and D^-. The larger the value is, the closer it is to the optimal level.

$$D^+ = \sqrt{\sum_{i=1}^{n} (V_{ij} - V_j^+)^2} \tag{15}$$

$$D^+ = \sqrt{\sum_{i=1}^{n} (V_{ij} - V_j^-)^2} \tag{16}$$

$$Score = \frac{D_i^-}{D_i^+ + D_i^-} \tag{17}$$

2.2 Indoor Experimental Method

In order to simulate the outdoor environment conditions in winter and test the ice melting performance of the pavement test specimen, it is necessary to adopt the test method of controlling a single variable while keeping other variables the same, so as to explore the influence of each variable on the ice-melting performance.

During the ice melting experiment, a custom-made ice layer was laid on the surface of the test specimen at a preset thickness (10 mm). Once the overall temperature stabilized to the predetermined constant level, power was supplied to the heating elements inside the specimen to monitor the melting process. The optimal heating structure layout was determined based on ice melting performance indicators, construction difficulty, and durability, which guided the structural design of the ice melting pavement. Concurrently, ice melting performance tests were conducted at varying temperatures (−5℃, −10℃, −15℃) and heating powers (350 W/m^2, 400 W/m^2, 500 W/m^2, 600 W/m^2), to determine the optimal heating power for the heating elements under different ambient temperatures.

2.3 Experimental Results and Discussion

2.3.1 Surface heat transfer and ice melting effect

Taking specimen A as an example, the heat transfer effect and melting effect of the specimen with the ambient temperature of −5℃ and heating wire power of 600 W/m^2 were studied over time, as shown in Fig.7 and Fig.8. The total ice melting time lasts three hours, with the first hour dedicated to preheating and the subsequent two hours for actual ice melting. As shown in the diagram, after one hour of power supply, the specimen's surface temperature reached the required melting threshold, though no visible changes occurred in the ice layer. At this stage, the average temperatures measured on the specimen surface and heating wires were 7.1℃ and 36.67℃ respectively. Turned on the power after two hours, initial melting of the ice layer began, with both temperatures raising to 8.1℃ and 42.12 ℃ respectively. After three hours of power application, complete ice melting was achieved, with the average temperatures raising further to 8.85℃ and 45.56℃ for both the specimen surface and heating wires.

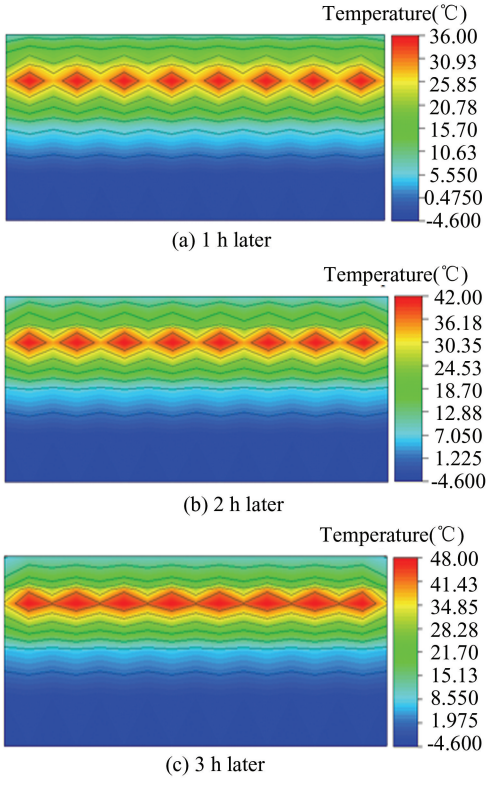

Fig.7 Thermal map of section of specimen A

Fig. 9 displays the temperature variation curves for measurement points 3 and 4 on the pavement surface of specimen A, as well as for points 13 and 15 in the thermal layer, and the temperature data collected at the bottom of specimen. The graph shows that after the preheating phase (0−3600s), surface temperatures stabilized. Notably, the temperature of specimen's bottom remained consistent with the

ambient temperature (−5℃), demonstrating that the thermal reflective film effectively blocked downward heat transfer and enhanced thermal energy utilization efficiency.

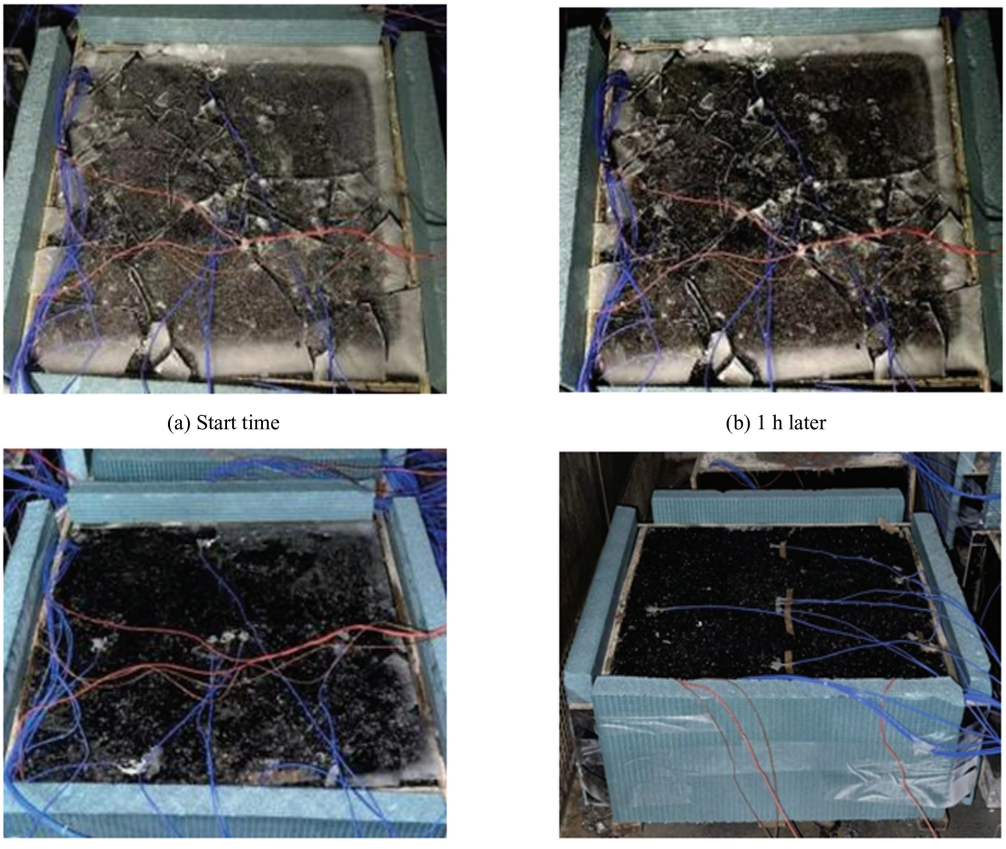

(a) Start time (b) 1 h later

(c) 2 h later (d) 3 h later

Fig.8 Ice melting process of specimen A

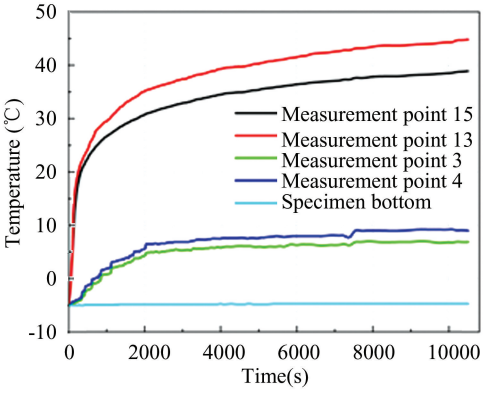

Fig. 9 Temperature variation with time at different measurement points

2.3.2 Effect of different heating wire spacing

The spacing of heating wire is closely related to the uniformity and raise of temperature, which directly affects the effect of ice melting. Under the test conditions of the same ambient temperature (−5 ℃), burial depth (50 mm) and heating wire power (600 W/m^2), the heating effect of heating wire and pavement is shown in Fig.10 under the three spacing sizes of 50mm (specimen C), 75mm (specimen A) and 100mm (specimen D). These conclusions can be drawn from Fig. 10: (1) The peak surface temperature of the concrete is concentrated above the heating element, with the adjacent gap area forming a low-temperature band; (2) The non-uniform property of the heat conduction path leads to a significant temperature gradient of the plate surface. When the heating element spacing was set at 100 mm, there was a significant difference in temperature uniformity compared to spacing of 75 mm and 50 mm. The isotherms showed extremely uneven density distribution with substantial temperature fluctuations, achieving a surface temperature standard deviation of 7.54, making it difficult to establish a stable and uniform thermal field. When the cable spacing was adjusted to 75 mm, the isotherms became more densely and uniformly distributed, with smoother

spatial temperature variations and significantly reduced inter-area temperature differences, achieving a surface temperature standard deviation of 5.69. When the cable spacing was further reduced to 50mm, the isotherms exhibited nearly uniform distribution, achieving high-level temperature uniformity across the entire pavement surface area. At this optimal spacing, the surface temperature standard deviation reached its minimum value of 4.32.

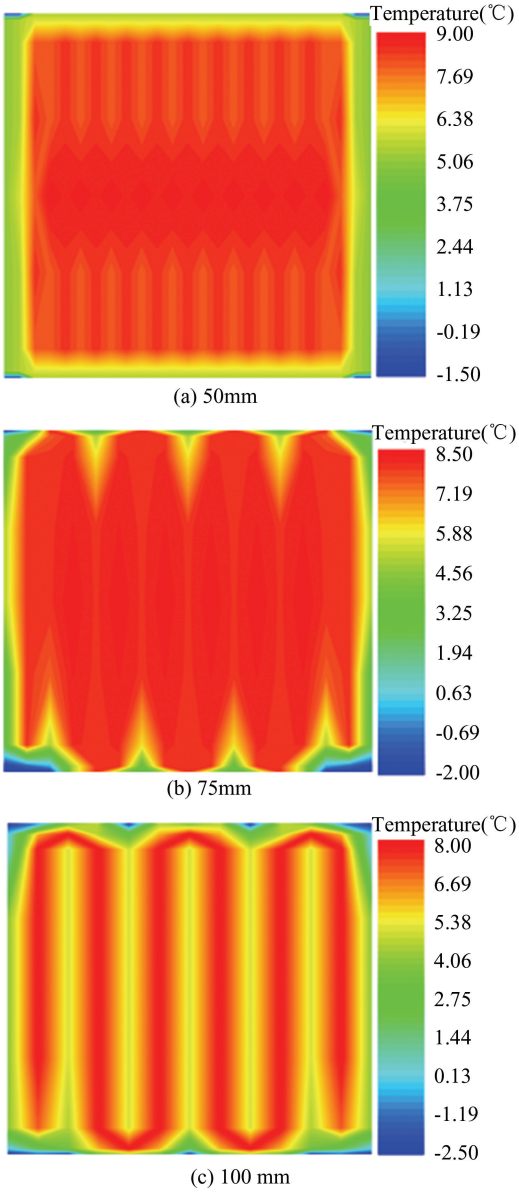

Fig.10 3D isotherm map of the surface of the road panel at different heating wire spacing

Taking specimens A, C and D as the objects, the surface temperature distribution of specimens, the temperature distribution of specimens in cross section, the snow-free area ratio A_r and the variation coefficient T_{cv} of temperature were studied under different spacing conditions, as shown in Fig. 11 and Fig. 12. As can be seen from Fig. 11, although there are obvious differences in the spacing of heating wires, the average temperature on the surface of pavement panel specimens is basically maintained at a similar level. This means that when these specific factors are fixed, the change of heating wire spacing does not cause significant fluctuation in the average temperature level, but it significantly affects the uniformity of surface temperature. As can be seen from Fig. 12, with the increase of layout spacing, A_r value and T_{cv} value show a gradual decreasing trend and an increasing trend respectively. The best melting effect is achieved when the layout spacing is 50mm, when the values of A_r and T_{cv} reach 0.92 and 0.48 respectively.

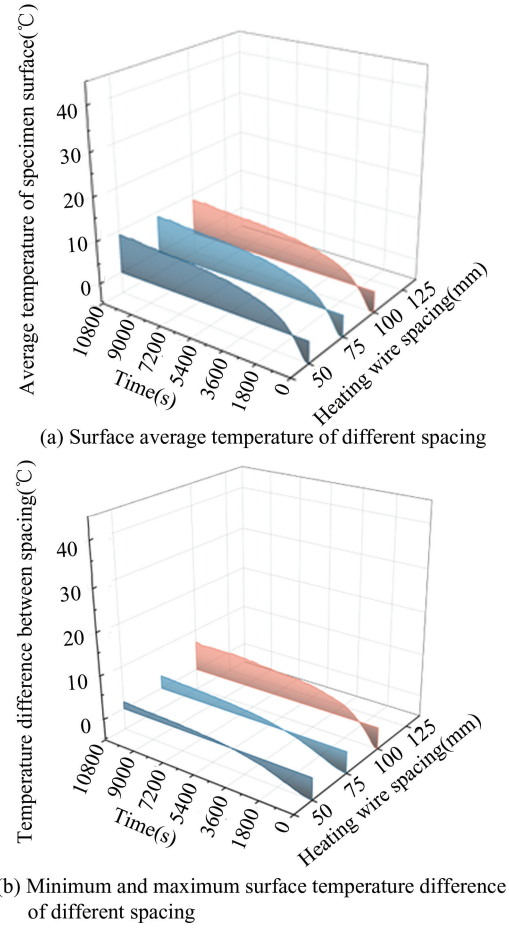

Fig.11 Temperature variation of different spacing

2.3.3 *Effect of different heating wire depth*

Using specimens A and B as test cases, this study investigated the effects of different burial depths on ice-melting performance under external

temperatures of −5℃ and a heating power of 600 W/m^2. The results are presented in Fig. 13 and Fig.14. Fig.13 indicates that adjusting the heating wire placement depth had relatively limited impact on the maximum stable temperature reached by the pavement slab specimens. Fig.14 shows that as the heating wire depth increased, the A_r values decreased while the T_{cv} values showed an upward trend. At the end of the experiment, the A_r values reached 0.88 and 0.92, with corresponding T_{cv} values of 0.64 and 0.48.

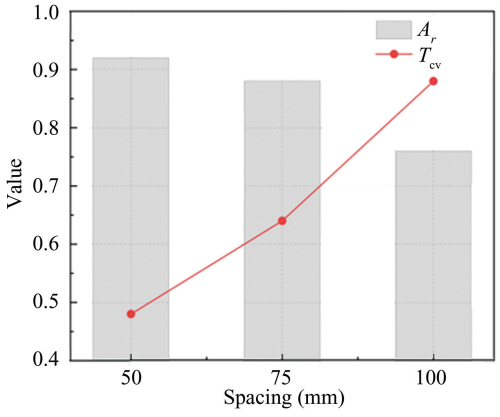

Fig.12 Changes of A_r and T_{cv} under different spacing

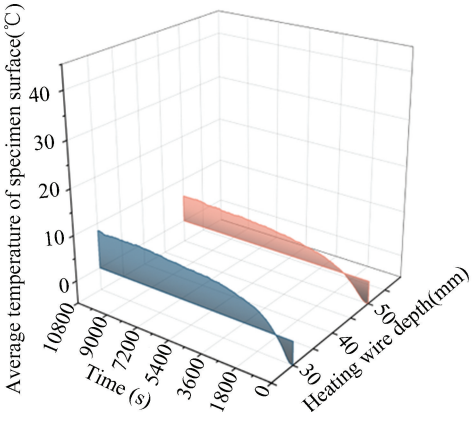

Fig.13 Average surface temperature of pavement panel specimens with different cable burial depths

2.3.4 *Effect of different heating wire power*

Taking specimen A as the object, the influence of different heating wire heating power on the effect of ice melting was studied at the ambient temperature of −5℃. The results are shown in Fig.15 and Fig.16. As can be seen from Fig. 15, under the same other conditions, the stable maximum temperature on the pavement surface and the stable maximum temperature of heating wire both increase significantly as the power increases. When the heating power of the wire is 350W/mm^2, 4000W/mm^2, 500W/mm^2, and 600W/mm^2 respectively, the surface temperatures of the test specimens reach 4.2℃, 4.8℃, 7.0℃, and 9.1℃. Therefore, the selection of specific power should be based on actual environmental conditions (such as ambient temperature). As shown in Fig. 16, with the increase in heating element power, the values of A_r and T_{cv} show a trend of gradual increase and decrease respectively.

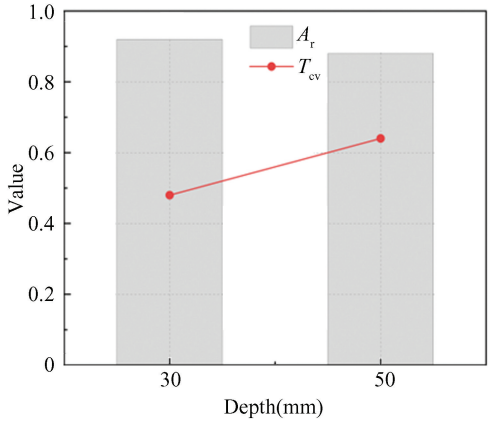

Fig. 14 Changes of A_r and T_{cv} under different burial depths

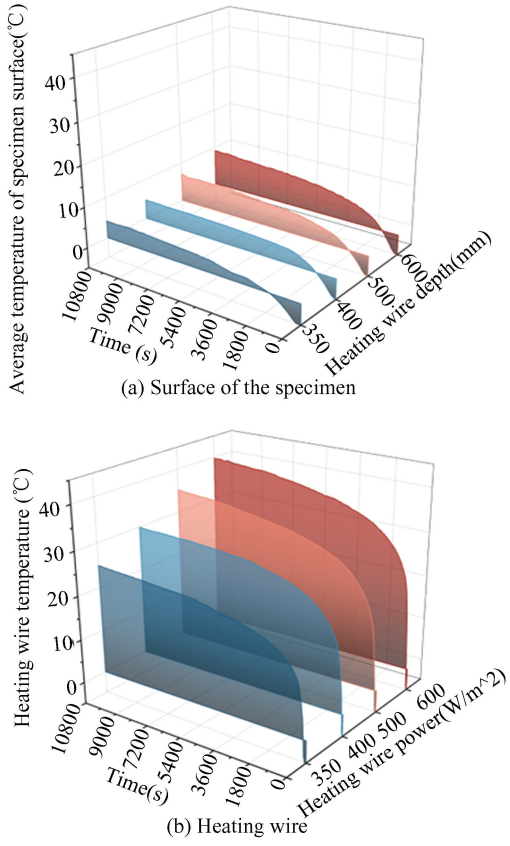

Fig.15 Temperature variation of different power

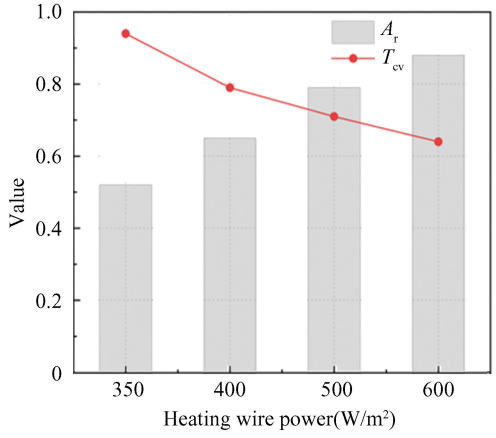

Fig.16 Variation of Ar and T_{cv} under different heating wire power

Taking specimen A as the object, the influence of heating wire power on melting effect at ambient temperature of −5℃, −10℃ and −15℃ was studied under 600 W/m^2, and the results are shown in Fig. 17 and Fig. 18. As shown in Fig.17, under the specific conditions of constant power per unit area, consistent burial depth of heating wires and the same spacing between heating wires, the fluctuation of ambient temperature has a significant impact on the temperature state of the surface of pavement panel specimens and heating wires. Moreover, a lower ambient temperature leads to a slower rate at which the pavement surface and heating wire reach their maximum stable temperature. It also results in a lower final stable temperature. As shown in Fig. 18, when ambient temperature exceeds −10℃, the heating element configuration of specimen A still achieves effective ice melting performance with A_r values consistently above 0.75 and T_{cv} values below 0.75. However, at −15℃, the A_r value drops to 0.64 while the road surface exhibits highly uneven temperature distribution. At this critical temperature threshold, the current spacing and burial depth configurations of the heating elements fail to meet ice melting requirements, necessitating either reduced spacing or installation depths.

Based on the results shown in Fig. 15−Fig. 18, the recommended optimal operational strategy is: Set the heating element power to 350 W/m^2 when ambient temperature exceeds −5℃; 400 W/m^2 when ambient temperature falls between −5℃ and −10℃; 500 W/m^2 when ambient temperature ranges from −10℃ to −15℃; and 600 W/m^2 when ambient temperature drops below −15℃.

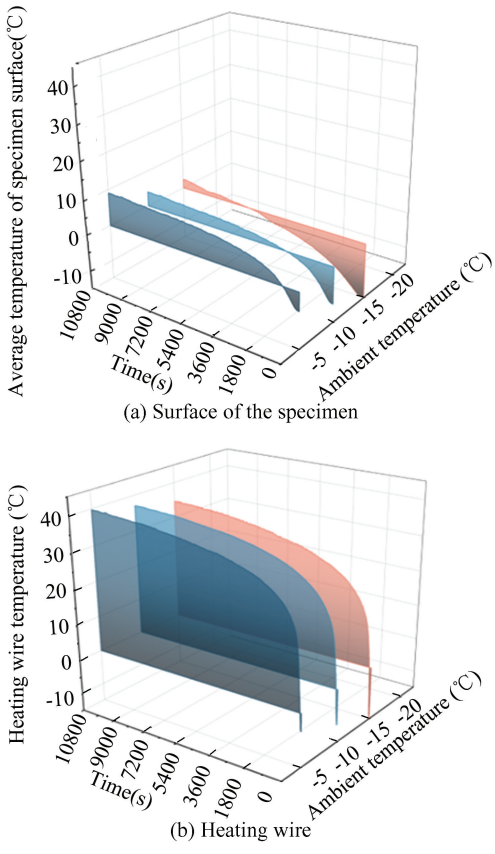

Fig.17 Temperature variation of different ambient temperature

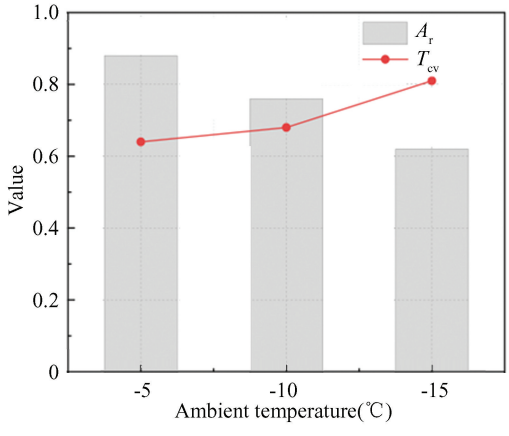

Fig. 18 Variation of A_r and T_{cv} under different ambient temperatures

2.4 Multi-Dimensional Comprehensive Evaluation

According to the above test methods and test results, six snowmelt performance indexes of specimens A−F are shown in Table 5. The data in the table indicates that while the heating wire achieves optimal ice melting efficiency at a depth of 30 mm with 50mm spacing. However, this configuration presents greater construction difficulty and durability.

To address these issues, this study employs the AHP-TOPSIS method to evaluate the snow-melting performance of layout scheme A-F, comprehensively considering factors such as melting efficiency, construction complexity, and structural durability.

Table 5 Data of ice melting performance index under different layout schemes

Specimen	A_r	μ	σ	T_{cv}	C_d	C_e
A	0.88	8.85	5.69	0.64	0.02	0.01
B	0.85	10.92	4.79	0.44	0.03	0.01
C	0.76	8.55	7.54	0.88	0.02	0.01
D	0.92	9.05	4.32	0.48	0.02	0.02
E	0.82	10.57	7.82	0.74	0.03	0.01
F	0.94	11.17	3.14	0.28	0.03	0.02

In order to determine the importance of different ice melting performance indicators, a judgment matrix was established between the indicators, as shown in Table 6. The judgment matrix shows the scaling of the importance of indicators by the size of the elements in the matrix. The value method of the elements in the matrix is shown in Table 7.

Table 6 The judgment matrix

Priority	A_r	μ	σ	T_{cv}	C_d	C_e
A_r	1	3	5	3	1/5	1/5
μ	1/3	1	2	2	1/5	1/5
σ	1/5	1/2	1	2	1/7	1/7
T_{cv}	1/3	1/2	1/2	1	1/3	1/3
C_d	5	5	7	3	1	1
C_e	5	5	7	3	1	1

Table 7 Construction method of judgment matrix

Scale	Meaning
1	It means that index *i* has the same importance as index *j*
3	It means that index *i* is slightly more important than index *j*
5	It means that index *i* is more important than index *j*
7	It means that index *i* is significantly more important than index *j*
9	It means that index *i* is extremely more than index *j*
2, 4, 6, 8	Represents the median value of the adjacent judgment above

The final calculation of the scores for layout schemes A-F is shown in Fig. 19. As can be seen from the figure, although scheme F has the best performance in ice melting effect, it ignores the construction difficulty and durability problems. After comprehensive consideration of various factors, scheme B is selected as the best layout scheme. According to calculation, the unit area production cost of specimen B is 308.98 yuan/m^2, and the maintenance cost is about 32.14 yuan/m^2 per year, which meets the cost requirements.

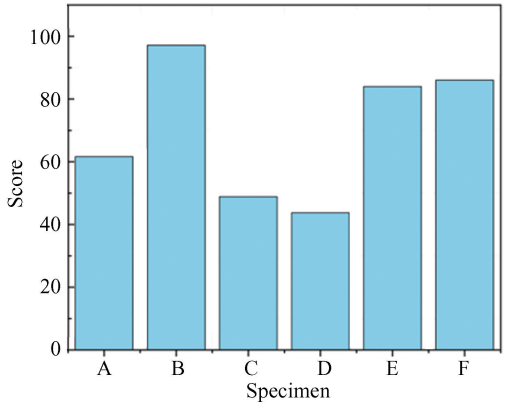

Fig.19 Score of scheme A-F

3 Outdoor Snow Melting Experiment

Based on the optimal pavement deicing layout parameters obtained in the above experiments, the outdoor deicing test section was set up to carry out the outdoor prefabricated asphalt concrete deicing test. This experiment aims to prove the superiority of prefabricated ice-melting pavement through practical application, accurately verify the effect of the arrangement scheme in actual engineering, further test the correctness of relevant theories, collect and analyze various data to quantify the effect of ice-melting from multiple dimensions.

3.1 The Processing of Specimen

The preparation of pavement panel specimen on the test section includes the following steps: (1) Make the pavement template to build the basic frame for subsequent construction; (2) Make the heating layer to ensure the realization of the ice melting function; (3) The temperature sensor is glued to monitor the temperature change in real time; (4) Apply mold release oil in the template and place the steel saddle to ensure the stability of the pavement structure; (5) Pour concrete base layer to consolidate the strength of pavement base; (6) Laying asphalt concrete on the surface of pavement structure; (7) The test site was arranged to make full preparations for the actual outdoor ice melting effect test in winter, and the test could be carried out when natural snow

fell. The finished specimen is shown in Fig.20.

Fig.20 The finished specimen

3.2 Outdoor Experimental Method

Based on the optimal pavement ice-melting layout parameters obtained from the above tests, pavement panel specimens with a size of 2400mm×1200mm×250mm were made, which is closer to the actual pavement in engineering. In the process of specimen making, according to the established scheme, the heating wire is laid with a depth of 30 mm and a spacing of 75mm to ensure that it is consistent with the optimal test scheme determined in Section 2.

Then, the outdoor snow melting test section was set up to carry out the outdoor snow melting test research. During the test, a professional camera is equipped to record the whole test process, and the environmental temperature, humidity and wind speed at corresponding moments are recorded. Through continuous recording and video recording for several hours, the melting process is observed.

During this phase, comprehensive data collection was conducted to quantitatively evaluate ice-melting effectiveness. Through practical field applications, the deployment plan's performance in real-world engineering scenarios was verified, further validating theoretical frameworks and providing robust data support for the widespread implementation of asphalt concrete pavement de-icing technology. The layout design of the outdoor test section is illustrated in Fig. 21.

3.3 Experimental Results

The average snow cover thickness on the day of the test was approximately 13mm (Fig. 22). The outdoor ice-melting experiment lasted 3 h (from 8:30AM to 11:30 AM), with an average outdoor temperature of −12℃, a snow cover thickness of 13 mm, and a controlled power output of 500 W/m^2.

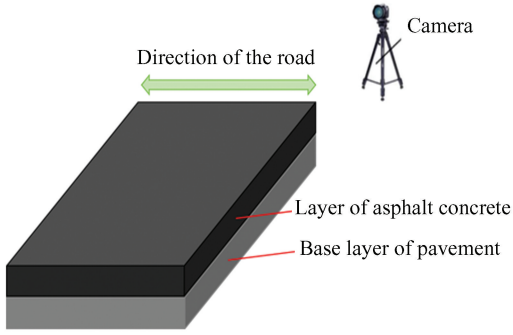

Fig.21 The layout scheme of the test section

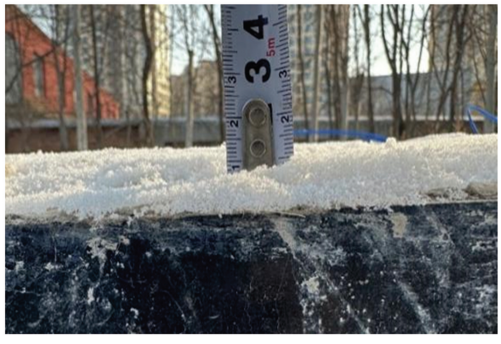

Fig.22 Snow thickness on pavement surface area

Fig. 23 shows the snow melting status of pavement panels at major time nodes during the whole three-hour ice melting process. The melting and snow conditions of pavement panels at major time nodes can be visually seen from the figures. Within the first hour after power activation, as shown in Fig.23 (a)−(b), the pavement slab enters a preheating phase where the snow surface remains unchanged. As illustrated in Fig.23 (b)−(d), during the 1 to 2−hour period after power supply, the preheating process concludes as the slab temperature stabilizing at its maximum achievable level, while the snow surface begins to show signs of melting. As shown in Fig.23 (d)−(f), the most significant snow melting effect occurred between 2 and 3 h, during which the snow removal operation was essentially completed. At 2.5 h, the pavement panels were in a state of ice and snow mixture. By the third hour, the remaining part was mainly ice formed by snow water produced by melting snow. At this time, the road surface condition had reached the level that did not affect traffic, which was in line with the expected effect of ice melting. In the final moment, the whole process of ice melting was completed, the value of *Ar* is about 0.943, which achieves superior snow melting effect.

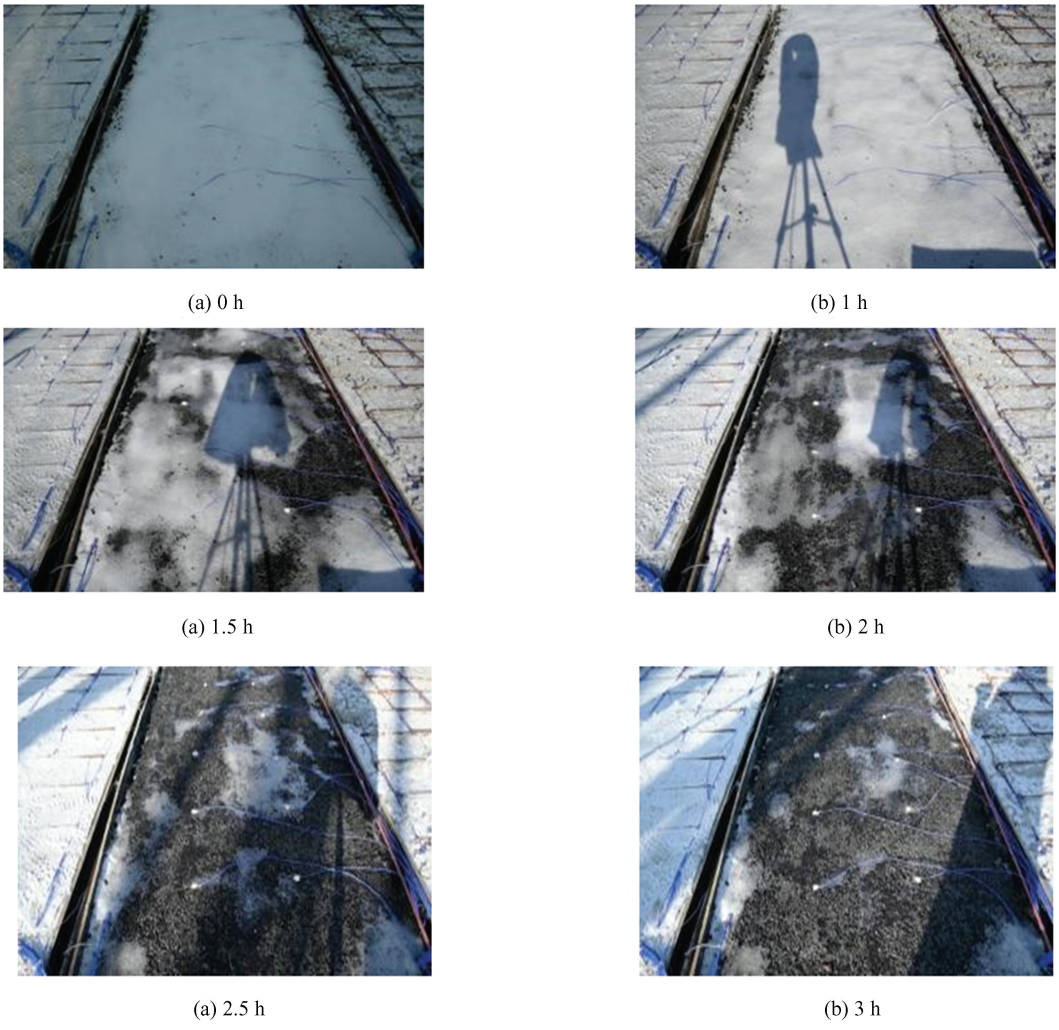

(a) 0 h (b) 1 h

(a) 1.5 h (b) 2 h

(a) 2.5 h (b) 3 h

Fig.23 The situation at each moment of the melting process

Fig.24 shows the temperature rise of the actual pavement panel deicing test in the first three hours. The temperature curve intuitively shows the dynamic change of the surface temperature of the pavement panel over time. With the progress of the test time, the surface temperature of the pavement panel shows a gradual upward trend and finally gets stabilized. The temperature curve of the heating wire showed that, in the initial stage of the test, the temperature rises rapidly and then also gets stabilized. According to the comprehensive observation of all the curves, the temperature of the heating wire rises rapidly in the initial stage of the test, and then enters a stable period. Meanwhile, the average temperature of the surface of the specimen is gradually increased under its influence, and finally reaches a relatively high stable value. Finally, the average temperature of the surface of the specimen reaches 2.225℃.

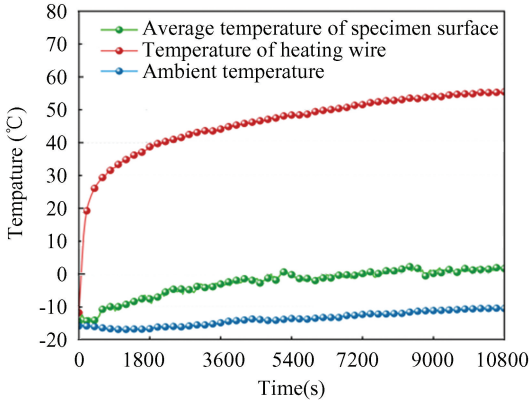

Fig.24 Time history of actual pavement plate snow melting test temperature

The thermal map of the final moment prefabricated pavement slab specimen is shown in Fig.25. As shown of the figure, the surface temperature of the specimen tends to be stable without

significant fluctuations. Due to the effect of the heat reflection film, the heat below the heating layer does not lose significantly. This uniform heat transfer process greatly improves the snow and ice melting performance of the prefabricated pavement.

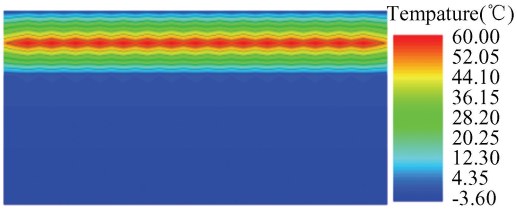

Fig. 25 Thermal map of section of pavement panel specimen

3.4 Analysis of Economic and Social Benefits

In addition to assessing whether the experimental road section's pavement meets technical requirements for effective snow and ice melting, its economic viability must also be evaluated, as this will determine the feasibility of scaling up and implementing the solution. Table 8 shows the material and labor costs for a carbon fiber heating wire with a burial depth of 30 mm and a spacing of 75 mm, as well as a pavement panel specimen measuring 2400 mm×1200 mm×250 mm. The final cost per square meter was 191.36 yuan, which is more cost-effective and simpler construction process than active ice-melting methods such as geothermal cycle systems[39], liquid heating systems[40]. At the same time, this technology effectively prevents the suboptimal performance of traditional snow removal and the corrosion of asphalt and roadbeds caused by de-icing agents in critical ice-snow disaster-prone areas such as bridges, long longitudinal slopes, tunnel entrances, airport runways, and highway hubs. It ensures smooth traffic flow on key road sections during winter and significantly enhances driving safety in snowy and rainy weather conditions.

Table 8 Economic cost of test specimen

Material	Unit price	Use level
48K carbon fiber heating cable	70 yuan/root	3 roots(12m/root)
Reinforcing bars	1.5 yuan/m	22.05m
Thermal reflective film	1.9 yuan/m^2	3.6m^2
C40 concrete	400 yuan/m^3	0.9m^3
Template	90 yuan	1 set
Total	—	688.89 yuan
Cost per square meter	—	191.36 yuan/m^2

4 Conclusions

In accordance with standard specifications, this study designed asphalt pavement ice-melting specimens featuring distinct configurations of heating elements. Comparative analysis of their ice melting performance identified optimal operational strategies across varying ambient temperatures. The AHP-TOPSIS method was employed to determine the optimal thermal source arrangement for heating elements. Based on these results, a prefabricated asphalt concrete ice melting pavement was developed. Subsequent snow melting tests conducted in cold outdoor environments yielded. The conclusions are as follows.

(1) Taking specimen A-F as the object, the ice melting effect under different heating wire spacing and burial depth was studied, and the melting performance indexes under various conditions were calculated, which provided basic data for confirming the optimal heating wire spacing.

(2) The prefabricated asphalt concrete ice melting pavement panels are manufactured in factories and transported to construction sites for installation, assembly, leveling, alignment, and locking. After all precast panels are installed and tested, the surface concrete is roughened to enhance friction, improve anti-slip and erosion resistance, and strengthen adhesion with the asphalt surface layer. Compared to traditional cast-in-place de-icing pavement construction methods, this prefabricated assembly approach minimizes heat source damage during installation while significantly boosting construction efficiency through optimized modular production.

(3) The ice melting performance of specimen A under varying ambient temperatures and heating wire power levels was analyzed to determine optimal operational strategies. The study revealed that: When ambient temperature exceeds −5℃, the heating wire should be set at 350 W/m^2; For temperatures between −5℃ and −10℃, adjust to 400W/m^2; At −10℃ to −15℃ ambient temperatures, increase to 500 W/m^2; Below −15℃ ambient temperature, set the heating wire power to 600W/m^2.

(4) The results of the comparison of the ice melting performance indexes of specimens A-F based on the AHP-TOPSIS method were evaluated, and the optimal arrangement of heating wire was obtained as 30mm burial depth and 75mm spacing.

(5) Based on the optimal heating element arrangement, a prefabricated ice-melting pavement panel specimen measuring 2400m×1200mm×250mm

was manufactured and subjected to outdoor testing. The final test results showed an average temperature of 2.31℃ and a snow-free area ratio Ar of approximately 0.943. These findings validate the rationality of the confirmed optimal heat source layout and operational strategy, demonstrating superior ice-melting performance while enabling rapid construction of prefabricated ice-melting pavements.

This study systematically investigates the ice melting performance of carbon fiber - reinforced asphalt concrete pavements. However, constrained by the current scarcity of physical engineering cases, the research faces limitations in conducting long - term analysis of ice melting effects and evaluating economic and social benefits. At the same time, the designed ice melting pavement can be linked to the development of smart cities and can be developed into a multifunctional road ice melting system in the future.

References

[1] Pan P, Wu Sh, Xiao Y, et al. A review on hydronic asphalt pavement for energy harvesting and snow melting. Renewable and Sustainable Energy Reviews, 2015, 48: 624-634. DOI: 10.1016/j.rser.2015.04.029.

[2] Ameri M, Sadeghiavaz M. Using magnetite filler to enhance the microwave healing of asphalt mixtures. Case Studies in Construction Materials, 2025, 22: e04341. DOI: 10.1016/j.cscm.2025.e04341.

[3] Kayaci N, Kanbur B B. Numerical and economic analysis of hydronic-heated anti-icing solutions on underground park driveways. Sustainability, 2023, 15(3): 2564. DOI: 10.3390/su15032564.

[4] Cui Y, Zhang F, Shao Y, et al. Techno-economic comprehensive review of state-of-the-art geothermal and solar roadway energy systems. Sustainability, 2022, 14(17): 10974. DOI: 10.3390/su141710974.

[5] Guo D, Sun X, Tian J, et al. Salt release and performance of self-ice-melting epoxy asphalt pavement under accelerated loading simulation conditions. Construction and Building Materials, 2025, 467: 140360. DOI: 10.1016/j.conbuildmat.2025.140360.

[6] Chen X, Huang G, Li Q, et al. A novel geothermal pavement ice and snow melting system with reversible loop heat pipes to eliminate underground thermal imbalance. Applied Thermal Engineering, 2025, 269 (part B): 126052. DOI: 10.1016/j.applthermaleng.2025.126052.

[7] Zhang Y, Shi X. Laboratory evaluation of a sustainable additive for anti-icing asphalt. Cold Regions Science and Technology, 2021, 189: 103338. DOI: 10.1016/j.coldregions.2021.103338.

[8] Zou G, Chen Q, Jiao Y, et al. Research on deicing performance of high-elastic/salt-storage asphalt mixture containing rubber particle and self-developed salt-storage filler. Construction and Building Materials, 2024, 449: 138303. DOI: 10.1016/j.conbuildmat.2024.138303.

[9] Wang X, Ma B, Li S, et al. Review on application of phase change materials in asphalt pavement. Journal of Traffic and Transportation Engineering (English Edition), 2023, 10(2): 185-229. DOI: 10.1016/j.jtte.2022.12.001.

[10] Zhang D, Bu W, Wang Q, et al. A review of recent developments and challenges of using phase change materials for thermoregulation in asphalt pavements. Construction and Building Materials, 2023, 400: 132669. DOI: 10.1016/j.conbuildmat.2023.132669.

[11] Jiao W, Sha A, Liu Z, et al. Study on thermal properties of steel slag asphalt concrete for snow-melting pavement. Journal of Cleaner Production, 2020, 277: 123574. DOI: 10.1016/j.jclepro.2020.123574.

[12] Lu D, Jiang X, Leng Z, et al. Electrically conductive asphalt concrete for smart and sustainable pavement construction: A review. Construction and Building Materials, 2023, 406: 133433. DOI: 10.1016/j.conbuildmat.2023.133433.

[13] Xu K, Chen Z, Xiao H, et al. Analysis of entransy dissipation thermal resistance and heat transfer efficiency of electrical heating snow-melting pavement. Thermal Science and Engineering Progress, 2025, 61: 103551. DOI: 10.1016/j.tsep.2025.103551.

[14] Liu K, Fu C, Xie H, et al. Design of electric heat pipe embedding schemes for snow-melting pavement based on mechanical properties in cold regions. Cold Regions Science and Technology, 2019, 165: 102806. DOI: 10.1016/j.coldregions.2019.102806.

[15] Mohammed A G, Ozgur G, Sevkat E. Electrical resistance heating for deicing and snow melting applications: Experimental study. Cold Regions Science and Technology, 2019, 160: 128-138. DOI: 10.1016/j.coldregions.2019.02.004.

[16] Wang F, Fu C, Liu K, et al. Experimental study and numerical simulation of concrete pavement electrical heating for snow melting. Construction and Building Materials, 2024, 442: 137611. DOI: 10.1016/j.conbuildmat.2024.137611.

[17] Hassan M A M. Investigation of performance of heat pipe as heat exchanger using alternative refrigerants. Journal of Energy Engineering, 2013, 139(1): 18-24. DOI: 10.1061/(asce)ey.1943-7897.0000091.

[18] Liu K, Huang S, Jin C, et al. Prediction models of the thermal field on ice-snow melting pavement with electric heating pipes. Applied Thermal Engineering, 2017, 120: 269-276. DOI: 10.1016/j.applthermaleng.2017.04.008.

[19] Lim H, Lee S, Lee J. Effective snow removal devices for road pavement using geothermal heat pipe. Applied Thermal Engineering, 2025, 265: 125624. DOI: 10.

1016/j.applthermaleng.2025.125624.
[20] Sadati S M S, Cetin K, Ceylan H, et al. Energy and thermal performance evaluation of an automated snow and ice removal system at airports using numerical modeling and field measurements. Sustainable Cities and Society, 2018, 43:238-250. DOI: 10.1016/j.scs.2018.08.021.
[21] Ma Z, Wei H, Wei D, et al. Heat transfer characteristics and preheating time prediction of conductive rubber active snow melting bridge deck. Applied Thermal Engineering, 2025,265:125604. DOI:10.1016/j.applthermaleng.2025.125604.
[22] Wang T, Abdallah M, Clevenger C, et al. Time-cost-quality trade-off analysis for planning construction projects. Engineering, Construction and Architectural Management, 2021, 28(1): 82-100. DOI: 10.1108/ECAM-12-2017-0271.
[23] Liu H, Maghoul P, Bahari A, et al. Feasibility study of snow melting system for bridge decks using geothermal energy piles integrated with heat pump in Canada. Renewable Energy, 2019, 136: 1266-1280. DOI: 10.1016/j.renene.2018.09.109.
[24] Rees S J, Spitle J D, Xiao X. Transient analysis of snow-melting system performance. ASHRAE Transactions, 2002, 108(2): 406-423.
[25] Liu X, Rees S J, Spitler J D. Modeling snow melting on heated pavement surfaces. Part I: Model development. Applied Thermal Engineering, 2007, 27(5-6): 1115-1124. DOI:10.1016/j.applthermaleng.2006.06.017.
[26] Liu X, Rees S J, Spitler J D. Modeling snow melting on heated pavement surfaces. Part II: Experimental validation. Applied Thermal Engineering, 2007, 27(5-6):1125-1131. DOI:10.1016/j.applthermaleng.2006.07.029.
[27] Liu K, Huang S, Xie H, et al. Multi-objective optimization of the design and operation for snow-melting pavement with electric heating pipes. Applied Thermal Engineering, 2017, 122: 359-367. DOI: 10.1016/j.applthermaleng.2017.05.033.
[28] Ma Z, Wei H, Wei D, et al. Study on snow melting performance evaluation and optimization design of conductive rubber electric heating pavement. Construction and Building Materials, 2025, 470: 140556. DOI: 10.1016/j.conbuildmat.2025.140556.
[29] Li H, Zhang Q, Xiao H. Self-deicing road system with a CNFP high-efficiency thermal source and MWCNT/cement-based high-thermal conductive composites. Cold Regions Science and Technology, 2013,86:22-35. DOI: 10.1016/j.coldregions.2012.10.007.
[30] Shi H, Xu H, Tan Y, et al. Multi-objective optimization of operation strategy in snow melting system for airfield runway using genetic algorithm: A case study in Beijing Daxing International Airport. Renewable Energy, 2022, 201(Part 2): 100-116. DOI: 10.1016/j.renene.2022.11.070.
[31] Jiao W, Sha A, Liu Z, et al. Utilization of steel slags to produce thermal conductive asphalt concretes for snow melting pavements. Journal of Cleaner Production, 2020, 261:121197. DOI: 10.1016/j.jclepro.2020.121197.
[32] Zou J, Gao Y, Liu Q, et al. Feasibility of a snow-melting membrane roof with an electrical-thermal system and prediction of its performance. Applied Thermal Engineering, 2023, 222: 119869. DOI: 10.1016/j.applthermaleng.2022.119869.
[33] Zhu X, Zhang Q, Du Z, et al. Snow-melting pavement design strategy with electric cable heating system balancing snow melting, energy conservation, and mechanical performance. Resources, Conservation and Recycling, 2022, 177:105970. DOI: 10.1016/j.resconrec.2021.105970.
[34] Zhang C, Tan Y, Chen F, et al. Long-term thermal analysis of an airfield-runway snow-melting system utilizing heat-pipe technology. Energy Conversion and Management, 2019, 186: 473-486. DOI: 10.1016/j.enconman.2019.03.008.
[35] Ministry of Transport of the People's Republic of China. Specifications for Highway Geometric Design, 2018, JTG D20—2017(EN).
[36] Han C, Yu X(Bill). Feasibility of geothermal heat exchanger pile-based bridge deck snow melting system: A simulation based analysis. Renewable Energy, 2017, 101: 214-224. DOI: 10.1016/j.renene.2016.08.062.
[37] Zou J, Sun X, Zhou H. Sensitivity analysis and practical application of an automatic snow-melting membrane roof. Cold Regions Science and Technology, 2023, 206: 103754. DOI: 10.1016/j.coldregions.2022.103754.
[38] Jalilibal Z, Amiri A, Castagliola P, et al. Monitoring the coefficient of variation: A literature review. Computers & Industrial Engineering, 2021, 161:107600. DOI: 10.1016/j.cie.2021.107600.
[39] Adebayo P, Jathunge C B, Darbandi A, et al. Development, modeling, and optimization of ground source heat pump systems for cold climates: A comprehensive review. Energy and Buildings, 2024, 320: 114646. DOI: 10.1016/j.enbuild.2024.114646.
[40] Chen H, Wu Y, Xia H, et al. Review of ice-pavement adhesion study and development of hydrophobic surface in pavement deicing. Journal of Traffic and Transportation Engineering (English Edition), 2018, 5(3):224-238. DOI: 10.1016/j.jtte.2018.03.002.
[41] Zhao H. Experimental Investigation on Concrete Pavement and Bridge Deck Deicing with Carbon Fiber Heating Wire. Dalian: Dalian University of Technology. 2020.